International Journal of Nanomedicine

Dovepress
open access to scientific and medical research

Open Access Full Text Article

ORIGINAL RESEARCH

Multifunctional organic–inorganic hybrid nanoparticles and nanosheets based on chitosan derivative and layered double hydroxide: cellular uptake mechanism and application for topical ocular drug delivery

This article was published in the following Dove Press journal:
International Journal of Nanomedicine
28 February 2017
Number of times this article has been viewed

Huibo Chi[1,2,*]
Yan Gu[1,*]
Tingting Xu[1]
Feng Cao[1]

[1]Department of Pharmaceutics, School of Pharmacy, China Pharmaceutical University, Nanjing, [2]State Key Laboratory of Drug Delivery Technology and Pharmacokinetics, Tianjin Institute of Pharmaceutical Research Co., Ltd., Tianjin, People's Republic of China

*These authors contributed equally to this work

Abstract: To study the cellular uptake mechanism of multifunctional organic–inorganic hybrid nanoparticles and nanosheets, new chitosan–glutathione–valine–valine-layered double hydroxide (CG-VV-LDH) nanosheets with active targeting to peptide transporter-1 (PepT-1) were prepared, characterized and further compared with CG-VV-LDH nanoparticles. Both organic–inorganic hybrid nanoparticles and nanosheets showed a sustained release in vitro and prolonged precorneal retention time in vivo, but CG-VV-LDH nanoparticles showed superior permeability in the isolated cornea of rabbits than CG-VV-LDH nanosheets. Furthermore, results of cellular uptake on human corneal epithelial primary cells (HCEpiC) and retinal pigment epithelial (ARPE-19) cells indicated that both clathrin-mediated endocytosis and active transport of PepT-1 are involved in the internalization of CG-VV-LDH nanoparticles and CG-VV-LDH nanosheets. In summary, the CG-VV-LDH nanoparticle may be a promising carrier as a topical ocular drug delivery system for the treatment of ocular diseases of mid-posterior segments, while the CG-VV-LDH nanosheet may be suitable for the treatment of ocular surface diseases.

Keywords: LDH nanoparticles, LDH nanosheets, ocular drug delivery, human corneal epithelial primary cell, retinal pigment cell, ARPE-19, active targeting

Introduction

Topical ophthalmic formulations have been widely used for their convenience, noninvasiveness and good patient compliance. Unfortunately, the low ocular bioavailability (<5%) due to the biopharmaceutical barriers significantly limits their therapeutic efficacy in ocular diseases.[1] In recent years, novel drug delivery strategies have been developed to improve the ocular bioavailability, especially for the posterior segment diseases. It has been shown that nanotherapies for the treatment of ocular diseases can efficiently improve the bioavailability by prolonging drug residence time on the ocular surface, as well as the permeability across the corneal and conjunctival epithelium.[2]

Layered double hydroxides (LDHs), a class of anionic clay materials, are found to be a potential inorganic nanocarrier for drug and gene delivery due to their large specific surface area (100–300 m^2/g),[3] high positive charge density (0.031–0.041 $e \cdot Å^{-2}$),[4] good biocompatibility[5] and low toxicity.[6] Today, organic–inorganic hybrid LDH nanocomposites have received extensive attention for numerous fields of applications owing to their

Correspondence: Feng Cao
Department of Pharmaceutics, School of Pharmacy, China Pharmaceutical University, 24 Tongjia Xiang, Nanjing 210009, People's Republic of China
Tel +86 25 8327 1092
Fax +86 25 8330 1606
Email cpufengc@gmail.com

submit your manuscript | www.dovepress.com
Dovepress
http://dx.doi.org/10.2147/IJN.S129311

unique properties. Organic–inorganic hybrid LDH nanocomposites consist mainly of three types, organic-coated inorganic hybrid LDH nanoparticles (Figure 1A), organic-intercalated inorganic hybrid LDH nanoparticles (Figure 1B) and organic–inorganic hybrid LDH nanosheets (Figure 1C).[7] Our previous studies showed that cross-linking polyvinylpyrrolidone (PVP)-coated LDH nanoparticles in ophthalmic solution could effectively increase the ocular retention time. The C_{max} and area under the concentration $(AUC)_{0-6\,h}$ of PVP-coated nanoparticle eye drops were 5.3- and 6.3-fold greater than those of commercial eye drops, respectively.[8] Pre-activated chitosan–glutathione (CG-2-Mercaptonicotinic acid [MNA]) and CG were synthesized and further used in the preparation of organic-intercalated inorganic hybrid LDH nanoparticles, which prolonged precorneal residence time successfully.[9] CG–valine–valine (CG-VV) was designed to form organic-intercalated inorganic hybrid LDH nanoparticles (CG-VV-LDH) with active targeting, which increased ocular retention time, enhanced corneal permeability and improved bioavailability.[10] Studies by other groups indicated that surface modification on LDH nanoparticles with amino or carboxyl could promote the delivery of LDH nanoparticles to targeted organs.[11] When LDH nanoparticles were delaminated into LDH nanosheets, the specific surface area was increased to 260–460 m^2/g.[12] Owing to the highly specific surface area, LDH nanosheets with higher drug adsorption and good surface activity attracted wide attention. Wang et al[13] showed that LDH nanosheets were efficient in gene delivery. Our recent studies suggested that sodium carboxyl methyl cellulose (CMCNa)-LDH nanosheets could prolong precorneal residence time significantly.[14] Li et al also showed that LDH nanosheets conjugated with folic acid could improve the therapeutic effect of methotrexate (MTX).[15] Both LDH nanoparticles and LDH nanosheets have been exploited for drug/gene delivery, but there is no study on the comparison of LDH nanoparticles with LDH nanosheets in vitro and in vivo.

Peptide transporter-1 (PepT-1), as an important membrane transporter for improving oral bioavailability, is mainly expressed in the small intestine epithelium.[16] In our previous work, prodrugs of oleanolic acid with better permeability and oral bioavailability were designed based on PepT-1-mediated active transport.[17,18] PepT-1 is also expressed on human corneal epithelial primary cells[19] (HCEpiC, representing native corneal epithelium) and retinal pigment epithelial cells[20] (ARPE-19, a popular cell line in the retinal pigment epithelium [RPE] cell research, representing retinal tissue in the posterior segment of eyes).[21] Our previous studies demonstrated an improved permeability of CG-VV-LDH nanoparticles across the cornea while experimenting with permeation behavior of isolated rabbit cornea. This effect may be due to the active transport of PepT-1.[10] However, there is no study on organic–inorganic hybrid LDH nanosheets with active targeting so far.

Pirenoxine sodium (PRN), the model drug of this study, is mainly used in the treatment of cataract to prevent denaturation of lens protein.[22] In our recent studies, eye drops using CG-VV-LDH nanoparticles have been evaluated systematically in vitro and in vivo except for cellular uptake mechanism.[10] In this study, new CG-VV-LDH hybrid nanosheets with active targeting to PepT-1 were prepared and characterized with laser particle sizer, zeta potential, X-ray diffraction (XRD) and transmission electron microscopy (TEM). In addition, stability, in vitro drug release, in vitro corneal penetration and in vivo precorneal retention of CG-VV-LDH nanosheets were analyzed systematically and further compared with

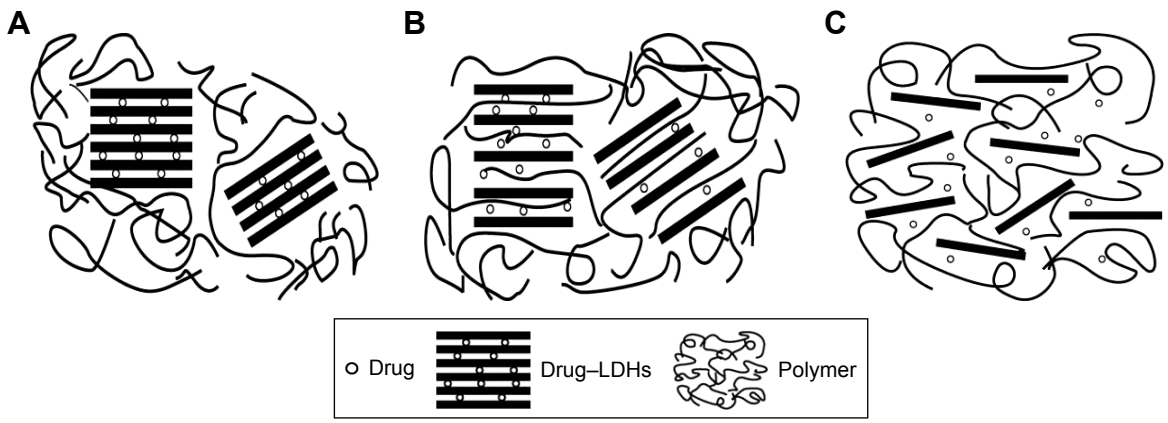

Figure 1 Diagrams of three types of organic–inorganic hybrid nanocomposites based on polymer, LDHs and drug.
Notes: (**A**) Organic-coated inorganic hybrid LDH nanoparticles. (**B**) Organic-intercalated inorganic hybrid LDH nanoparticles. (**C**) Organic–inorganic hybrid LDH nanosheets.
Abbreviation: LDH, layered double hydroxide.

those of CG-VV-LDH nanoparticles. Finally, these two types of nanocomposites were compared with respect to their cytotoxicity, cellular uptake and uptake mechanism on HCEpiC and ARPE-19 cells for the first time.

Materials and methods

Materials and animals

Zinc L-lactate was purchased from Aike Reagent Company (Sichuan, China). Aluminum lactate and fluorescein isothiocyanate (FITC) isomer I were obtained from Sigma-Aldrich Trading Co., Ltd. (Shanghai, China). PRN was provided by Chengdu Sino-Strong Pharmaceutical Co., Ltd. (Sichuan, China). PRN eye drops were supplied by Hubei Yuanda Everyday Bright Eyes Pharmaceutical Co. Ltd. (Hubei, China; specification: 15 mL, 0.8 mg; batch number: 131038018). 3-(4,5-dimethyl-2-thiazolyl)-2,5-diphenyl-2-*H*-tetrazolium bromide (MTT), chlorpromazine hydrochloride, nystatin, genistein and amiloride were purchased from Aladdin Reagent Database Inc. (Shanghai, China). Gly-Sar was obtained from TCI Development Co., Ltd. (Shanghai, China). All other reagents were of high-performance liquid chromatography (HPLC) or analytical grades.

Male New Zealand albino adult rabbits were procured from the Qinglongshan farms in Jiangning District of Nanjing and housed in standard cages with controlled temperature and humidity. They were fed with a standard laboratory chow and water ad libitum. All animal experiments were carried out according to the National Institutes of Health guide for the care and use of laboratory animals and approved by the Animal Ethical Experimentation Committee of China Pharmaceutical University.

Cell culture of HCEpiC and ARPE-19 cells

Cell culture of HCEpiC

Culture flasks (Thermo Fisher Scientific, Waltham, MA, USA) were pre-coated with poly-L-lysine at a concentration of 2 μg/cm^2 at least 1 h at 37°C before cell seeding. HCEpiC (Cat No 6510; ScienCell Research Laboratories, Carlsbad, CA, USA) were cultured in corneal epithelial cell serum-free medium (ScienCell Research Laboratories) supplemented with 1% corneal epithelial cell growth supplement and 1% penicillin/streptomycin solution. Cells were incubated in a humidified atmosphere containing 5% CO_2 at 37°C according to ScienCell Research Laboratories' protocol.

Cell culture of ARPE-19 cells

ARPE-19 cells (Cat No ZQ0460; ScienCell Research Laboratories) were cultured in Dulbecco's Modified Eagle's Medium (DMEM/Nutrient Mixture F-12, Wisent Biotechnology Co, Ltd, Nanjing, China) supplemented with 10% fetal bovine serum (FBS; ScienCell Research Laboratories) and 1% penicillin/streptomycin solution. The environment of cell incubation was the same with HCEpiC.

Synthesis of LDH nanoparticles, CG-VV-LDH nanoparticles, PRN-LDH nanoparticles, CG-VV-PRN-LDH nanoparticles, FITC-LDH nanoparticles, CG-VV-FITC-LDH nanoparticles, CG-VV-FITC solution and FITC solution

CG-VV was synthesized previously by our group.[10] LDH nanoparticles, PRN-LDH nanoparticles, CG-VV-PRN-LDH nanoparticles, FITC-LDH nanoparticles and CG-VV-FITC-LDH nanoparticles were prepared using coprecipitation method as published recently.[10,23] Furthermore, 1 mL of FITC solution (1 mg/mL) was added in 4 mL of CG-VV solution (475 μg/mL) as the control solution (CG-VV-FITC solution, 0.0038 mg/mL) of CG-VV-FITC-LDH nanoparticles. FITC (1 mg) was dissolved in 1 mL of dimethyl sulfoxide (DMSO) as FITC solution.

Synthesis and characterization of LDH, CG-VV-LDH and CG-VV-PRN-LDH nanosheets

Synthesis of LDH nanosheets, CG-VV-LDH nanosheets, CG-VV-PRN-LDH nanosheets, CG-VV-FITC-LDH nanosheets and CG-VV-FITC solution

The Zn, Al-lactate, HCO_3-LDHs were synthesized using a coprecipitation method as reported previously.[24] $Zn(C_3H_5O_3)_2$ (0.913 g) and $Al(C_3H_5O_3)_3$ (0.368 g) were dissolved in 100 mL of deionized water and mixed slowly with 100 mL of $NaHCO_3$ solution (5.25%, w/v). NaOH solution (2 M) was added dropwise to the mixture until the pH value reached 8.0±0.1. The resultant suspension was aged for 12 h at room temperature, then centrifuged (10,000 rpm, 10 min) and washed five times with deionized water. For the preparation of LDH nanosheets, LDH slurry was resuspended in 50 mL of deionized water, followed by homogenization (20,000 rpm, 2 min) using a homogenizer (F6/10-8G; Fluko, Shanghai, China) until no sediment was observed. A small amount of coexistent HCO_3 ions would disrupt the orderly arrangement of interlayer lactate ions, which facilitate the delamination of layers in water at room temperature without heating or ultrasonication. Finally, the white suspension was stirred constantly at room temperature for 8 h until the solution became transparent.

CG-VV-LDH nanosheets were prepared by adding 1 mL of LDH nanosheets (1 mg/mL) dropwise into 1 mL

of CG-VV solution (4 mg/mL) under vigorous stirring. Then, the mixture was stirred for 1 h to ensure full adsorption. CG-VV-PRN-LDH nanosheets were prepared by adding 167 μL of 1 mg/mL PRN solution into 1 mL of CG-VV-LDH nanosheet suspension. The suspension was then stirred for 1 h to ensure complete PRN adsorption onto LDH nanosheets. CG-VV-FITC-LDH nanosheets were prepared by adding 50 μL of FITC solution (2 mg/mL) to 1 mL of CG-VV-LDH nanosheets (0.5 mg/mL) under vigorous stirring for 1 h at room temperature and away from light. Then, 0.2 mL of FITC solution (0.02 mg/mL) was added in 0.8 mL of CG-VV solution (1 mg/mL) as the control solution (CG-VV-FITC solution, 0.8 mg/mL) of CG-VV-FITC-LDH nanosheets.

Physiochemical properties of LDH, CG-VV-LDH and CG-VV-PRN-LDH nanosheets

Particle size and zeta potential of LDH, CG-VV-LDH and CG-VV-PRN-LDH nanosheets were measured using ZetaPlus analyzer (Brookhaven Instruments Corporation, Holtsville, NY, USA) by dynamic light scattering (DLS). XRD patterns were recorded by D/max-2500/PC X-ray diffractometer (Rigaku, Tokyo, Japan) with Cu Kα radiation (λ=0.154 nm) in the range of 2°–70° with a scanning speed of 2°/min at 40 kV and 40 mA. XRD samples of LDH nanosheets, CG-VV-LDH nanosheets and CG-VV-PRN-LDH nanosheet colloidal suspensions were transparent glue-like aggregate collected by centrifuging at 12,000 rpm for 30 min. The samples for morphological observation of LDH nanosheets and CG-VV-LDH nanosheets were dropped on the surface of a copper grid without being stained or dried and further observed by JEM-200CX TEM (JEOL Ltd, Tokyo, Japan).

Drug-loading efficiency of CG-VV-PRN-LDH nanosheets was measured by dialysis method. A certain amount of CG-VV-PRN-LDH nanosheet suspension was pipetted into a dialysis bag (molecular weight cutoff [MWCO] of 8–14 kDa) and dialyzed against deionized water overnight. Subsequently, the suspension was transferred to a volumetric flask, mixed with 1 mL of hydrochloric acid (HCl, 5 M) and diluted with DMSO to volume. The concentration of PRN was determined by HPLC (LC-2010CHT; Shimadzu, Kyoto, Japan). Drug-loading efficiency was calculated as the amount of PRN determined divided by the amount of total PRN.

In vitro drug release of CG-VV-PRN-LDH nanosheets

Drug release characteristic of CG-VV-PRN-LDH nanosheets in vitro was determined using dynamic dialysis method. In brief, 1 mL of PRN solution or CG-VV-PRN-LDH nanosheets containing 50 μg of PRN was transferred into a dialysis bag (MWCO of 8–14 kDa), placed in phosphate-buffered saline (PBS; pH 7.4) at 35°C±0.5°C and gently shaken at 400 rpm. Then, 0.5 mL of dissolution medium was collected at specific intervals (10, 30, 45, 60, 90, 120, 180, 240, 300, 360, 480 and 720 min), filtrated through a 0.22 μm microporous filter and replaced with an equal volume of PBS to keep the volume constant. The concentration of PRN was measured by HPLC quantitatively.

Preparation and preliminary stability assessment of CG-VV-PRN-LDH nanosheet eye drops

The preparation of CG-VV-PRN-LDH nanosheet eye drops was as follows: glucose (6%, w/v) as an osmotic pressure regulator and trichlorobutanol (0.25%, w/v) as a preservative were added into 30 mL of CG-VV-PRN-LDH nanosheet suspension (50 μg/mL PRN). The pH of CG-VV-PRN-LDH nanosheet eye drops was in the range of 7.0–7.4.

To assess the preliminary stability of eye drops, CG-VV-PRN-LDH nanosheet eye drops were stored at room temperature for 10 days. Particle size, zeta potential, pH and the drug content of eye drops were measured at 0, 5 and 10 days.

In vivo precorneal residence behavior study

Six male New Zealand albino rabbits were randomly assigned into two groups equally. Approximately 50 μL of CG-VV-PRN-LDH nanosheet eye drops or commercial PRN preparation containing 2.5 μg PRN was administered into the lower conjunctival sac of the right eye of each rabbit by a micropipette. At specific intervals following the administration (10, 30, 60, 90, 120, 180, 240, 300 and 360 min), 10 μL of tear fluid samples was collected into centrifuge tube using a capillary and 90 μL of methanol was added to precipitate protein. Samples were vortexed for 10 min and centrifuged at 10,000 rpm for 10 min. Approximately 20 μL of the supernatants was injected into the HPLC. The linear regression equation for PRN in tear samples ranging from 0.1 to 10 μg/mL was A =10576C +94, R^2=0.9999, where C is the concentration of PRN in tear fluid samples.

In vitro corneal permeation test

The corneal permeation test in vitro was performed using Franz diffusion cells according to the method reported previously.[25] Briefly, the freshly excised rabbit cornea was mounted in Franz diffusion cell. The glutathione-sodium

bicarbonate Ringer's (GBR) solution filled in the thermostated (35°C±0.5°C) receptor chamber was stirred at 350 rpm. Then, 0.5 mL of commercial PRN or CG-VV-PRN-LDH nanosheet eye drops was gently added into the donor chamber. At specified intervals (30, 60, 90, 120, 180, 240 and 300 min), 0.5 mL of samples was collected from the receptor chamber and replaced immediately with an equal volume of GBR solution. The concentration of PRN was determined by HPLC.

Cytotoxicity assay of HCEpiC and ARPE-19 cells

Cytotoxicity assay of HCEpiC

Cell viability was determined by the MTT assay. Cell suspension was seeded in 96-well plates at a density of 2×10^4 cells/well and incubated for 48 h. Cell culture medium was removed and replaced with 200 µL of fresh medium containing LDH nanoparticles, CG-VV-LDH nanoparticles, LDH nanosheets or CG-VV-LDH nanosheets at the concentration of LDH ranging from 25 to 200 µg/mL for 12 h. Subsequently, the medium with LDH was aspirated and cells were rinsed twice with Dulbecco's PBS (DPBS; HyClone) carefully to remove the culture medium. Then, 180 µL of fresh medium and 20 µL of MTT (5 mg/mL, in pH 7.4 DPBS) were added to each well and incubated for 4 h at 37°C. Afterward, the medium was aspirated carefully and the formazan crystals were dissolved by adding 150 µL of DMSO to each well. The absorbance was measured at a wavelength of 570 nm using microplate reader (Multiskan FC; Thermo Scientific). Cell viability was calculated using the following equation:

$$\text{Cell viability} = \frac{OD_{sample} - OD_0}{OD_{control} - OD_0} \times 100\%$$

where OD is optical density, and OD_{sample} is the absorbance of cells treated under various conditions, $OD_{control}$ is the absorbance of cells cultured in medium without LDH and OD_0 is the absorbance of wells without cells.

Cytotoxicity assay of ARPE-19 cells

Cell suspension was seeded in 96-well plates at a density of 10^4 cells/well and incubated for 24 h. Cell culture medium was removed and replaced with 200 µL of fresh serum-free medium containing LDH nanoparticles, CG-VV-LDH nanoparticles, LDH nanosheets or CG-VV-LDH nanosheets at the concentration of LDH ranging from 25 to 200 µg/mL for 12 h. Subsequently, the medium with LDH was aspirated and the cells were rinsed twice with PBS (Hyclone) carefully to remove the culture medium. Other details of this assay and calculation of cell viability were the same as mentioned earlier.

Cellular uptake study

Inverted fluorescence microscope observation

For cellular uptakes, HCEpiC were seeded in 24-well plates at a density of 5×10^4 cells/well and incubated for 6 days. The medium was refreshed every 2 days. Then, the cells were incubated with 0.5 mL of medium containing FITC, CG-VV-FITC solution (3.8×10^{-4}% or 0.008% [w/v] CG-VV) or FITC-labeled LDH nanoparticles (2 µg/mL FITC) for 1, 2 and 4 h at 37°C, washed three times with DPBS and observed by inverted fluorescence microscope (Nikon, Tokyo, Japan).

ARPE-19 cells were seeded in 24-well plates at a density of 5×10^4 cells/well and incubated for 2 days. To facilitate the observation of fluorescence, the concentration of FITC was increased to 4 µg/mL. The following steps were the same as mentioned earlier except that ARPE-19 cells were rinsed with PBS.

Quantitative determination of intracellular PRN at different periods of time

HCEpiC were seeded in a 24-well plate (5×10^4 cells/well) and incubated for 6 days at 37°C. Subsequently, cells were exposed to PRN, CG-VV-PRN (3.8×10^{-4}% or 0.008% [w/v] CG-VV), PRN-LDH nanoparticles, CG-VV-PRN-LDH nanoparticles or CG-VV-PRN-LDH nanosheets (2 µg/mL PRN) for 1, 2 and 4 h at 37°C, respectively. Once the uptake was finished, the cells were rinsed twice with cold DPBS, trypsinized and resuspended in an appropriate volume of cold DPBS. Intracellular PRN concentration was measured by HPLC. Total protein concentration of cell samples was determined using the BCA assay kit (Cat No KGP905; KeyGen BioTech). The concentration of protein was calculated and calibrated with a standard curve ($y = 0.001x + 0.139$, $R^2 = 0.9977$, where y is the absorption measured at a wavelength of 570 nm using a microplate reader, x is the concentration of standard bovine serum albumin solution ranging from 25 to 500 µg/mL). The uptake index (UI) was calculated using the following formula of UI = C/P, where C is the concentration of PRN and P is the concentration of protein in cell samples.

Flow cytometry analysis

HCEpiC were seeded in a 12-well plate at a density of 10^5 cells/well and incubated for 6 days. The medium was

refreshed every 2 days. The cells were pre-incubated with sodium azide (2 mg/mL), hypertonic sucrose (0.45 M), chlorpromazine (10 μg/mL), nystatin (5 μg/mL), genistein (50 μg/mL), amiloride-HCl (10 μM) or Gly-Sar (1 mM, 5 mM, 10 mM) at 37°C for 30 min. The cells were then incubated with FITC-LDH nanoparticles, CG-VV-FITC-LDH nanoparticles or CG-VV-FITC-LDH nanosheets (2 μg/mL FITC) at 37°C for 4 h. After incubation, cells were rinsed twice with cold DPBS, trypsinized and finally resuspended in an appropriate volume of DPBS at concentrations ranging from 5×10^5 to 1×10^6 cells/mL. The fluorescence intensity was measured at excitation–emission wavelengths of 495/525 nm by MACSQuant Analyzer (Miltenyi Biotec, Cologne, Germany).

ARPE-19 cells were seeded in a 12-well plate at a density of 10^5 cells/well and incubated for 5 days. The medium was refreshed once during 5 days. Other details of this assay were the same as mentioned earlier except that the concentration of FITC was increased to 4 μg/mL. Serum-free medium and cold PBS were used in the subsequent steps.

Statistical analysis

All experiments were conducted at least in triplicate; data were presented as mean ± standard deviation (SD). Statistical analysis was performed using Origin software. Comparisons between groups were made using one-way analysis of variance (ANOVA) with Student's *t*-test. A *P*-value of <0.05 was considered statistically significant.

Results and discussion

Synthesis and characterization of LDH nanosheets

The synthesis and characterization of LDH nanoparticles are mentioned in the article recently published by our group.[10] Zn-Al-lactate, HCO_3-LDHs suspension was white and opaque (Figure S1A). After stirring for 8 h at room temperature, the suspension became a translucent colloidal dispersion which showed an obvious Tyndall effect (Figure S1B). The mean size of LDH nanosheets was 47.5±12.1 nm and polydispersity index was 0.210±0.021. LDH nanosheets possessed a high positive zeta potential of ~35.4±0.9 mV.

XRD is an important method for identifying structures of LDH nanosheets and LDH nanoparticles.[4] To confirm that Zn-Al-LDH nanoparticles have been delaminated into individual nanosheets, the structure of LDH nanosheets was characterized by XRD. The XRD pattern of Zn-Al-LDH nanoparticles (Figure S2A) shows sharp and symmetric (00*l*) Bragg reflections, suggesting LDH nanoparticles are crystalline layered compounds. The basal spacing of Zn-Al-LDH nanoparticles was ~7.65 Å corresponding to (003) diffraction peak. In comparison, the XRD pattern of exfoliated LDH nanosheets (Figure S2B) at low diffraction peak disappeared, indicating that Zn-Al-LDH nanoparticles lost their ordered layered structure and were delaminated into nanosheets. In addition, the morphology of LDH nanosheets was visualized by TEM. TEM images (Figure S3A) show that LDH nanosheets have an irregular shape (hexagon, circle or ellipse) and small particle size. These results further demonstrated that Zn-Al-LDH nanoparticles have been delaminated into nanosheets.

Synthesis and characterization of CG-VV-LDH and CG-VV-PRN-LDH nanosheets

The removal of organic solvent, the presence of electrolytes or drying can result in an immediate restacking of the exfoliated LDH nanosheets. The instability of LDH nanosheets is a great challenge which limits the application of LDH nanosheets. In the previous studies, CMCNa,[26] alginate[27] and albumin[28] were added into LDH nanosheets to prevent the restacking of LDH nanosheets. Our group also prepared CMCNa-LDH nanosheet eye drops which prolonged precorneal residence successfully.[14] In this study, CG-VV was introduced into the colloid as a stabilizing agent by encapsulating nanosheets instead of destroying the colloidal state.

The influence of the CG-VV/LDH mass ratio on the particle size, zeta potential and colloidal stability of CG-VV-LDH nanosheets was examined. As the CG-VV/LDH mass ratio increased from 1:1 to 8:1, the mean size of CG-VV-LDH nanosheets increased from 81.7 to 162.2 nm and meanwhile the zeta potential of CG-VV-LDH slightly increased (Table 1). When the ratio of CG-VV/LDH was 4:1, CG-VV-LDH hybrid nanosheets remained stable and well dispersed in PBS within 24 h. However, when the ratio of CG-VV/LDH decreased below 4:1, the particle

Table 1 Characterization of different types of CG-VV-LDH nanosheets

m(CG-VV): *m*(LDH)	Size (nm)	PI	Zeta potential (mV)
0:1	47.5±12.1	0.210±0.021	+35.4±0.9
1:1	81.7±2.4	0.230±0.011	+39.3±4.0
2:1	84.6±1.9	0.197±0.009	+50.4±4.4
4:1	102.8±2.7	0.252±0.013	+51.4±4.3
8:1	162.2±5.9	0.705±0.031	+45.1±2.8

Note: Each value represents mean ± SD (n=3).
Abbreviations: CG-VV, chitosan–glutathione–valine–valine; LDH, layered double hydroxide; PI, polydispersity index; SD, standard deviation.

size of CG-VV-LDH nanosheets increased, suggesting that the nanosheets aggregated in the presence of electrolytes (Figure S4). Considering the size, zeta potential and colloidal stability of CG-VV-LDH hybrid nanosheets, the optimum ratio of CG-VV/LDH was chosen as 4:1.

CG-VV-LDH hybrid nanosheet colloidal suspension was translucent. XRD pattern showed that the typical diffractions of LDH structure could not be observed (Figure S2C). The absence of 00*l* diffractions suggested that LDH nanosheets could attach to the surface of CG-VV and remained in a stable exfoliated state. Moreover, it could be seen from TEM images that CG-VV-LDH nanosheets are well dispersed without aggregation and have similar size and morphology with LDH nanosheets (Figure S3B).

Due to the high charge density and large specific surface area of LDH nanosheets, the drug-loading capacity of nanosheets is much larger than that of LDH nanoparticles. To ensure the stability of LDH nanosheets, the drug loading of LDH nanosheets was chosen as ~14%. After dialysis overnight, the drug efficiency of CG-VV-PRN-LDH nanosheets was 99.42%±0.21%, suggesting that PRN could be completely adsorbed on LDH nanosheets when the mass ratio of PRN to LDH nanosheets was 1:6. XRD pattern showed that the typical diffractions of LDH structure at a low angle could not be observed (Figure S2D), which is similar to that of CG-VV-LDH nanosheets. Therefore, LDH nanosheets can load PRN in a stable colloid at the mass ratio of PRN to LDH nanosheets of 1:6.

In vitro drug release of CG-VV-PRN-LDH nanosheets

The electrostatic adsorption of PRN on LDH nanosheets would easily lead to aggregation of the colloidal in artificial tears. Instead of artificial tears, PBS (pH 7.4) was used as release medium in vitro. The drug release profile of PRN solution and CG-VV-PRN-LDH nanosheet suspension in PBS (pH 7.4) is shown in Figure 2. The release of PRN solution was rapid and reached ~100% within 2 h. However, a sustained release of PRN from CG-VV-PRN-LDH nanosheets reached 74.6% over a period of 12 h. The release mechanism of CG-VV-PRN-LDH nanosheets was ion exchange: anions in release medium exchange with PRN which was adsorbed on the LDH nanosheets by electrostatic interaction. In our previous study, the drug release of CG-VV-PRN-LDH nanoparticles in artificial tears was almost 60% within 6 h.[10] Both CG-VV-PRN-LDH nanosheets and CG-VV-PRN-LDH nanoparticles showed a sustained release of PRN.

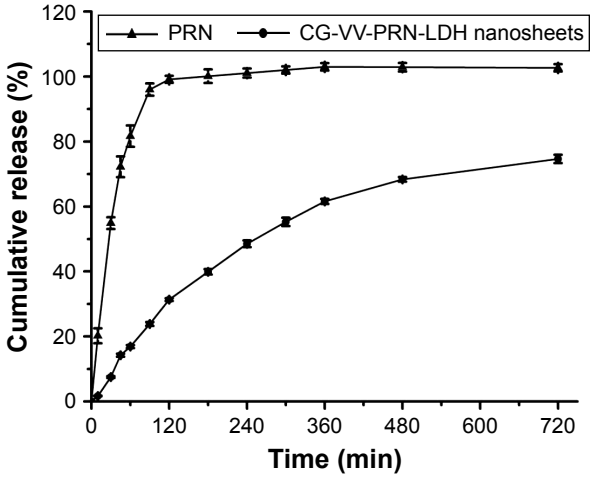

Figure 2 Cumulative release–time profiles of PRN and CG-VV-PRN-LDH nanosheets.
Note: Each value represents mean ± SD (n=3).
Abbreviations: PRN, pirenoxinesodium; CG-VV, chitosan–glutathione–valine–valine; LDH, layered double hydroxide; SD, standard deviation.

Preliminary stability assessment of CG-VV-PRN-LDH hybrid nanosheet eye drops

As given in Table 2, there is no obvious change in particle size, zeta potential, pH and the content of CG-VV-PRN-LDH nanosheet eye drops, while in storage for 10 days at room temperature indicating that the eye drops showed good stability during 10 days.

In vivo precorneal residence behavior study

The concentration–time profile of PRN in tear fluids is shown in Figure 3, and the main pharmacokinetic parameters are presented in Table 3. Following the administration of commercial PRN eye drops, the concentrations of PRN could be detected by HPLC for only 2 h, suggesting that PRN was eliminated rapidly from tears. In comparison, CG-VV-PRN-LDH nanosheet eye drops showed greater sustained drug release in the rabbit eyes where PRN could be detected up to 6 h. The $AUC_{0-6\,h}$ and mean retention time (MRT) of CG-VV-PRN-LDH hybrid nanosheet eye drops exhibited 5.1- and 1.9-fold increase compared with those of commercial PRN eye drops ($P<0.01$), respectively. Moreover, the clearance (CL) in tears of CG-VV-PRN-LDH hybrid nanosheets was significantly decreased ($P<0.01$). The results indicated that CG-VV-PRN-LDH nanosheet eye drops could greatly prolong the precorneal residence time. As our previous report, $AUC_{0-6\,h}$ and MRT of CG-VV-PRN-LDH nanoparticle eye drops exhibited 6.3- and 2.1-fold increase compared with those of commercial PRN eye drops, respectively.[10] Despite the difference in structure, these two types of LDH

Table 2 Stability of CG-VV-PRN-LDH nanosheet eye drops

Time (days)	Appearance	Particle size (nm)	Zeta potential (mV)	pH	Content (%)
0	No precipitation	108.4±2.1	+46.1±0.3	7.38±0.11	99.4±0.2
5	No precipitation	109.7±3.7	+43.8±0.8	7.45±0.14	99.1±0.8
10	No precipitation	106.1±1.9	+46.0±0.6	7.38±0.07	98.1±0.4

Notes: Each value represents mean ± SD (n=3). pH, hydrogen ion concentration.
Abbreviations: CG-VV, chitosan–glutathione–valine–valine; PRN, pirenoxine sodium; LDH, layered double hydroxide; SD, standard deviation.

nanocomposites with similar particle size and positive surface charge can prolong the retention time on the ocular surface. It can be explained by the interaction of the cysteine of sticky protein on cornea and free thiol groups on the chitosan derivative, resulting in bioadhesive ability of LDH nanocomposites. However, these two types of nanocomposites were positively charged, so they can combine with corneal epithelium through electrostatic attraction. Thus, eye drops using CG-VV-LDH hybrid nanosheets/nanoparticles with longer retention time can reduce the loss of drugs on the ocular surface in comparison with commercial eye drops.

In vitro corneal permeation test

In vitro corneal permeation profiles of commercial PRN and CG-VV-PRN-LDH nanosheet eye drops are illustrated in Figure 4. The cumulative permeation of CG-VV-PRN-LDH nanosheet eye drops during 5 h had no significant difference from that of commercial PRN eye drops. However, according to our previously reported study,[10] the cumulative penetration of CG-VV-PRN-LDH nanoparticle eye drops was ~5.2-fold higher than that of the commercial product.

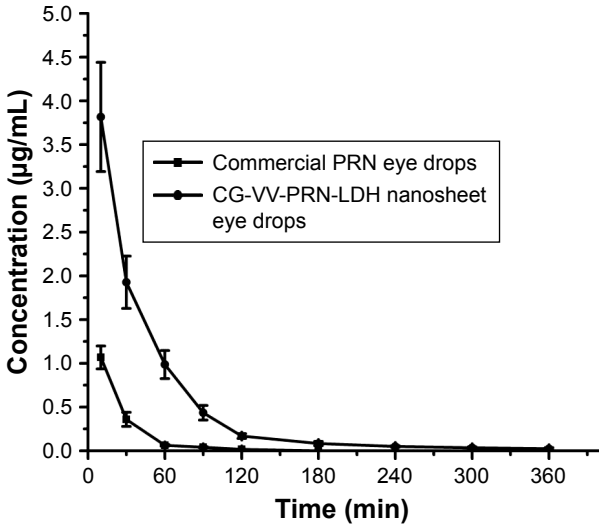

Figure 3 The concentration–time curve of PRN in tear samples of commercial PRN eye drops and CG-VV-PRN-LDH nanosheet eye drops.
Note: Each value represents mean ± SD (n=6).
Abbreviations: PRN, pirenoxine sodium; CG-VV, chitosan–glutathione–valine–valine; LDH, layered double hydroxide; SD, standard deviation.

The results suggested that CG-VV-PRN-LDH nanosheets play limited roles in the enhancement of corneal penetration, while CG-VV-PRN-LDH nanoparticles could significantly promote the corneal penetration of PRN. It is of some interest to find that the permeability of CG-VV-PRN-LDH nanosheets was significantly different from that of CG-VV-PRN-LDH nanoparticles even though both of them exhibited high cellular uptake in HCEpiC in the following studies. However, HCEpiC cannot mimic the whole cornea of animal which is composed of lipophilic epithelium, hydrophilic stroma and lipophilic endothelium.[29] In addition, CG-VV-PRN-LDH nanosheets are held together by electrostatic adsorption, whose transport mechanism across ocular tissues is different from that of CG-VV-PRN-LDH nanoparticles. Based on studies of in vivo precorneal residence and in vitro corneal permeation, CG-VV-PRN-LDH nanosheets are more suitable for the treatment of ocular surface diseases.

Cytotoxicity assay

The cell viability of HCEpiC was measured after incubation with various blank carriers and corresponding PRN-loaded formulations for 12 h. Cytotoxicity of LDH is strongly dependent on the concentration and physicochemical parameters of nanoparticles such as particle size, zeta potential, specific surface area and chemical composition. CG-VV-LDH nanoparticles and CG-VV-LDH nanosheets were characterized with similar particle size and zeta potential (133.2±11 nm, 31.9±1.3 mV; 108.4±2.8 nm, 45.3±0.76 mV, respectively). Whether LDH is intercalated with PRN or not, a high degree of cell viability (>85%) was exhibited at the concentration of LDH ranging from 0 to 75 μg/mL (Figure 5A and C), while a higher concentration of LDH may cause adverse effects.

The cell viability of ARPE-19 cells was also measured after incubation with various delivery carriers for 12 h. As shown in Figure 5B, the cytotoxicity of LDH was concentration dependent, which was consistent with the cytotoxicity study on HCEpiC mentioned earlier. Compared with HCEpiC, low cell viability was exhibited in ARPE-19 cells, probably because ARPE-19 cells are more sensitive to LDH.

Table 3 Pharmacokinetic parameters of commercial PRN eye drops and CG-VV-PRN-LDH nanosheet eye drops

Sample	$AUC_{0-6\ h}$ (μg/mL min)	MRT (min)	CL (mL/min)
Commercial PRN eye drops	34.05±3.13	18.69±3.68	0.074±0.007
CG-VV-PRN-LDH nanosheet eye drops	172.88±24.67**	34.62±1.93**	0.015±0.002**

Notes: Each value represents mean ± SD (n=6). **$P<0.01$ vs commercial PRN eye drops group.
Abbreviations: PRN, pirenoxine sodium; CG-VV, chitosan–glutathione–valine–valine; LDH, layered double hydroxide; $AUC_{0-6\ h}$, area under the concentration vs time curve from 0 to 6 h; MRT, mean retention time; CL, clearance; SD, standard deviation.

It is generally accepted that the safety concentration of LDHs as drug delivery carriers is <100 μg/mL.[30] Combining the cytotoxicity assay of HCEpiC and ARPE-19 cells, we considered an LDH concentration of <75 μg/mL to be a safe level for further experiments in this study. It is worth noting that LDHs, as a class of inorganic carriers, show greater toxicity than organic carriers (liposome,[31] micelle,[32] etc.) although the biocompatibility of LDH nanocomposites is better than that of carbon nanotubes[33] for the application of ocular drug delivery.

Cellular uptake studies

Cellular uptake was evaluated by inverted fluorescence microscope observation. The concentration of FITC for cellular uptake on HCEpiC was 2 μg/mL, but it was increased to 4 μg/mL for cellular uptake on ARPE-19 cells to facilitate the observation. As shown in Figure 6, the fluorescence intensity of cells increased with incubation time prolonging from 1 to 4 h, suggesting that the uptake of CG-VV-FITC-LDH nanoparticles and CG-VV-FITC-LDH nanosheets by HCEpiC and ARPE-19 cells was dependent on exposure time. The fluorescence microscopy images showed that cells treated with free FITC exhibited negligible fluorescence (Figure 6f). As shown in Figure 6d and e, the weak fluorescence of CG-VV-FITC suggested that CG-VV could slightly increase the uptake. FITC-LDH nanoparticles (Figure 6a) and CG-VV-FITC solution (0.00038%; Figure 6e) were control groups of CG-VV-LDH nanoparticles (Figure 6b). The differences between these three groups showed that the cellular uptake of CG-VV-LDH nanoparticles was the combined effect of CG-VV and LDH nanoparticles. Similarly, as shown in Figure 6c and d, CG-VV and LDH nanosheets functioned together for the cellular uptake of CG-VV-LDH nanosheets. HCEpiC treated with CG-VV-FITC-LDH nanoparticles exhibited much stronger fluorescence than CG-VV-FITC-LDH nanosheets after 4 h (Figure 6A) even though the content of CG-VV in CG-VV-LDH hybrid nanosheets was ~21 times higher than that in CG-VV-LDH hybrid nanoparticles. In fluorescence microscopy images of ARPE-19 cells (Figure 6B), CG-VV-FITC-LDH nanoparticles showed no superiority in cellular uptake compared with CG-VV-FITC-LDH nanosheets.

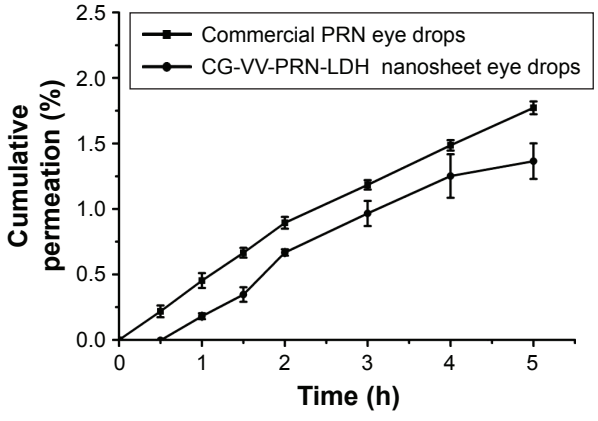

Figure 4 In vitro corneal permeation profiles of commercial PRN eye drops and CG-VV-PRN-LDH nanosheet eye drops in GBR solution.
Note: Each value represents mean ± SD (n=6).
Abbreviations: PRN, pirenoxine sodium; CG-VV, chitosan–glutathione–valine–valine; LDH, layered double hydroxide; GBR, glutathione-sodium bicarbonate Ringer; SD, standard deviation.

To study the cellular uptake profile of nanoparticles, intracellular PRN content was determined at different time points by HPLC. Quantitative analysis results showed that the cellular UI of PRN-LDH nanoparticles and CG-VV-PRN-LDH nanoparticles and CG-VV-PRN-LDH nanosheet group at 4 h was up to 1.6-, 2.9- and 2.1-fold higher than that of free PRN group, respectively. Furthermore, CG-VV-PRN-LDH nanoparticles exhibited nearly 40% higher cellular uptake than that of CG-VV-PRN-LDH nanosheets after 4 h of incubation (Figure S5), indicating improved cellular uptake efficacy of CG-VV-FITC-LDH nanoparticles.

To further study the cellular uptake mechanism of nanocomposites, HCEpiC and ARPE-19 cells were pre-incubated with specific inhibitors of endocytosis pathways for 30 min and co-incubated with FITC-labeled nanocomposites for 4 h. Cellular uptake of FITC-LDHs nanoparticles, CG-VV-FITC-LDH nanoparticles and CG-VV-FITC-LDH nanosheets at 4°C was significantly inhibited in comparison with that at 37°C, suggesting that an energy-dependent uptake process was involved in the internalization of nanocomposites. After incubation with sodium azide, a general inhibitor of cell energy metabolism, the cellular uptake decreased which indicated

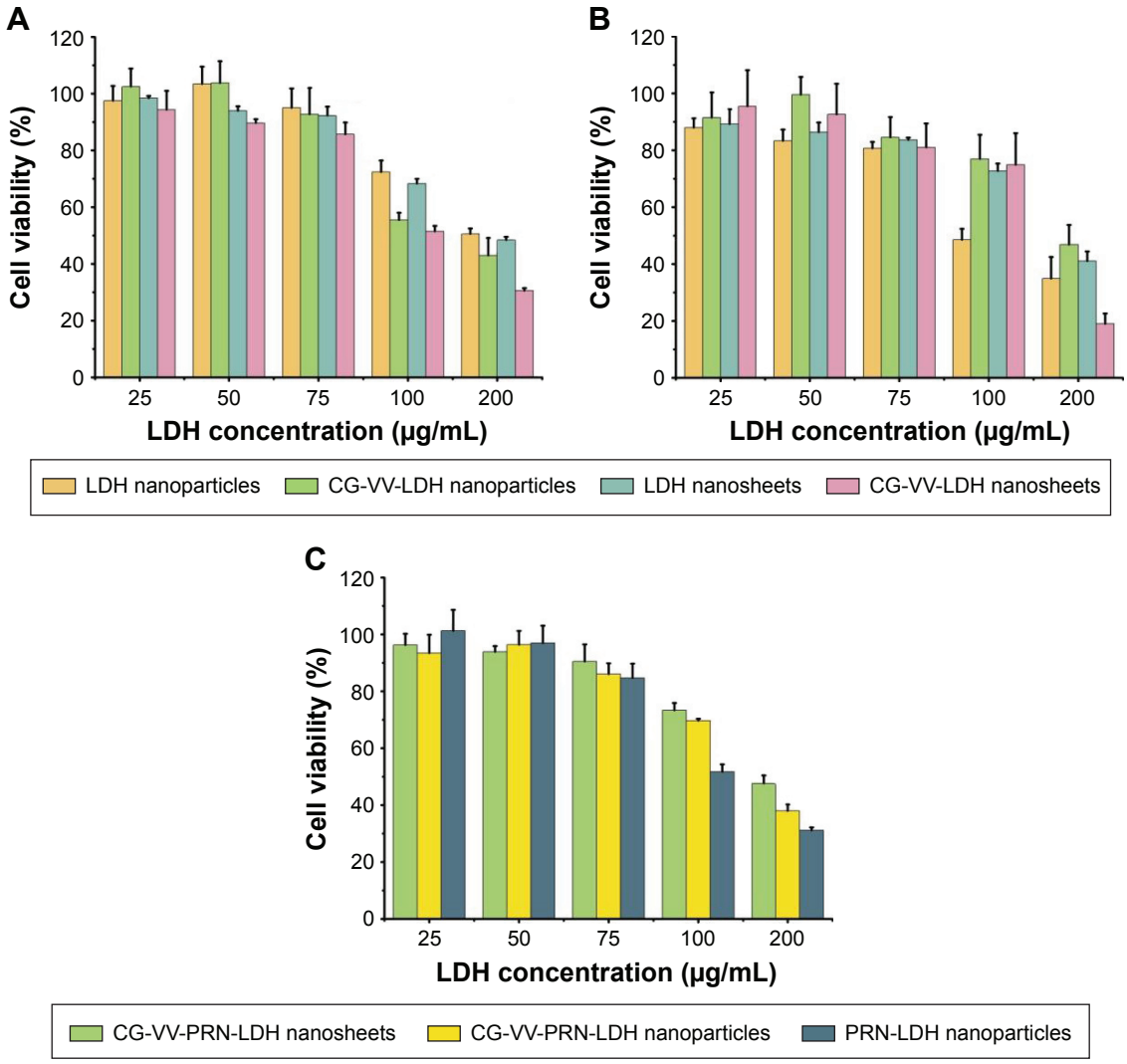

Figure 5 In vitro cytotoxicity of LDH nanoparticles, LDH nanosheets, CG-VV-LDH nanoparticles and CG-VV-LDH nanosheets against (**A**) HCEpiC, (**B**) ARPE-19 cells; (**C**) in vitro cytotoxicity of PRN-LDH nanoparticles, CG-VV-PRN-LDH nanoparticles and CG-VV-PRN-LDH nanosheets against HCEpiC after 12 h incubation, respectively; cell viability was determined by MTT assay.

Note: Each value represents mean ± SD (n=4).

Abbreviations: LDH, layered double hydroxide; CG-VV, chitosan–glutathione–valine–valine; HCEpiC, human corneal epithelial primary cells; ARPE-19, retinal pigment epithelial; PRN, pirenoxine sodium; MTT, 3-(4,5-dimethyl-2-thiazolyl)-2,5-diphenyl-2-*H*-tetrazolium bromide; SD, standard deviation.

that cellular internalization was an energy-dependent pathway. In addition, other inhibitors were further investigated to explain the uptake pathways (Figure 7). Hypertonic sucrose and chlorpromazine are inhibitors of clathrin-mediated endocytosis. Cellular uptake of nanoparticles in the presence of hypertonic sucrose and chlorpromazine significantly decreased ($P<0.01$) compared with the control group, respectively. Nystatin and genistein are known to inhibit the caveolae-mediated pathway, which had no significant influence on the cellular uptake. The macropinocytosis inhibitor amiloride had no effect on cellular uptake. These results indicated that clathrin-mediated endocytosis was involved in the internalization of nanocomposites, which was consistent with Xu et al's[34] studies on NIH 3T3 cells and Oh et al's[35] studies on MNNG/HOS cells. Moreover, to verify whether the uptake of CG-VV-LDHs nanoparticles and CG-VV-LDH nanosheets are specific to PepT-1 expressed on the cell membrane, competitive inhibition experiments were conducted by pre-incubating HCEpiC and ARPE-19 cells with a range of concentration of Gly-Sar. Gly-Sar was first evaluated for its effects on cell viability by MTT assay, and the results showed no cytotoxicity even at a concentration of 10 mM (Figure S6). The uptake of CG-VV-FITC-LDHs nanoparticles and CG-VV-FITC-LDH nanosheets in the presence of 1 mM Gly-Sar was similar to that of the control group. However, for HCEpiC, the uptake of CG-VV-FITC-LDHs nanoparticles was significantly inhibited ($P<0.05$) by 5 and 10 mM Gly-Sar, while the uptake of CG-VV-FITC-LDH nanosheets was inhibited

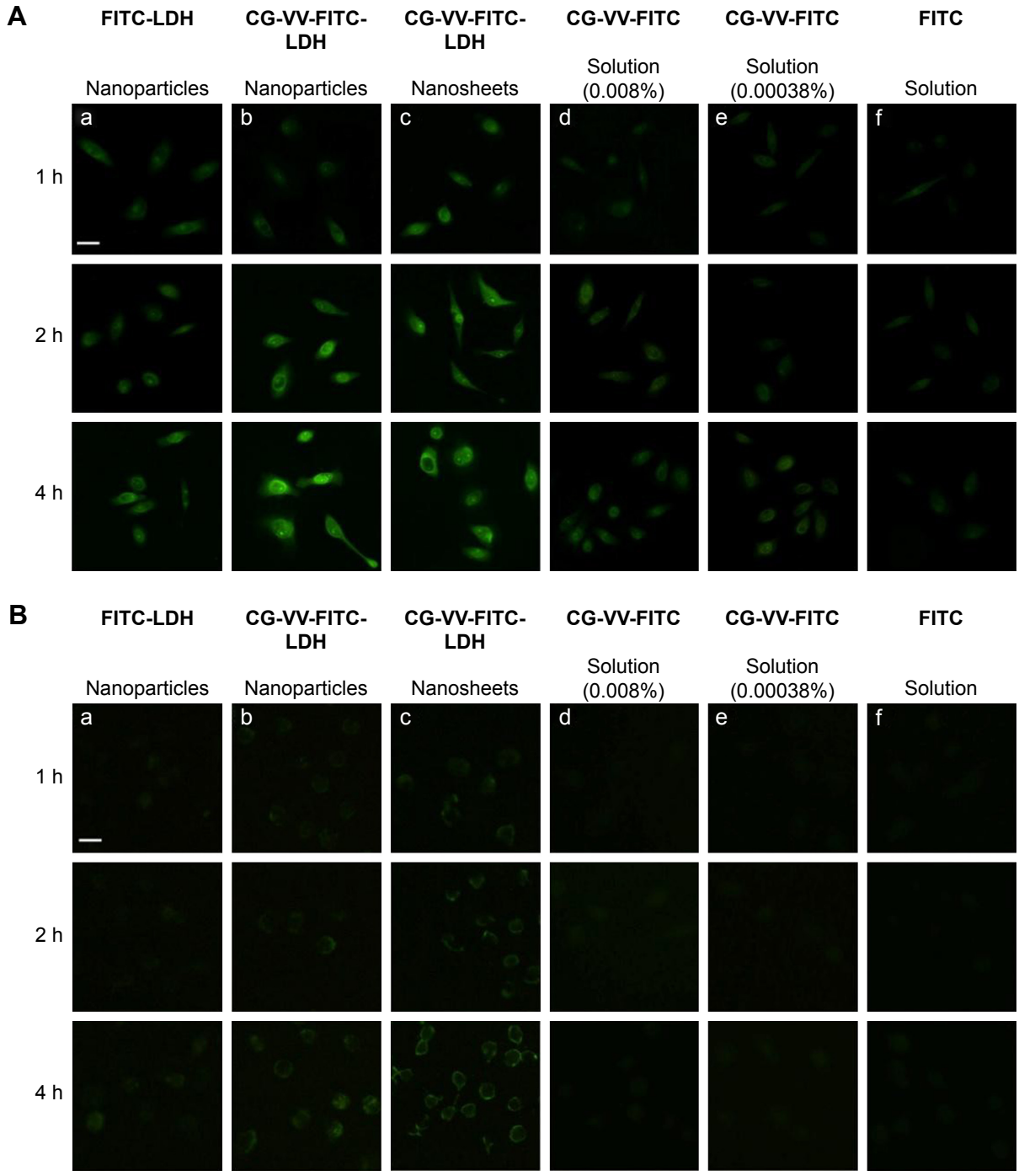

Figure 6 Fluorescence microscopy images of (**A**) HCEpiC and (**B**) ARPE-19 cells incubated with the following: a, FITC-LDH nanoparticles; b, CG-VV-FITC-LDH nanoparticles; c, CG-VV-FITC-LDH nanosheets; d and e, CG-VV-FITC solution (0.008% and 0.00038% [w/v]); f, free FITC at 37°C for 1, 2 and 4 h, respectively.
Note: Scale bar =25 μm.
Abbreviations: HCEpiC, human corneal epithelial primary cells; ARPE-19, retinal pigment epithelial; FITC, fluorescein isothiocyanate; LDH, layered double hydroxide; CG-VV, chitosan–glutathione–valine–valine.

until the concentration of Gly-Sar was 10 mM. For ARPE-19 cells, the uptake of CG-VV-FITC-LDHs nanoparticles and CG-VV-FITC-LDH nanosheets were both inhibited until the concentration of Gly-Sar was 10 mM (Figure 7A and B). It suggested that PepT-1 also mediated internalization. Based on these results, both clathrin-mediated endocytosis and active transport of PepT-1 participate in the internalization of CG-VV-LDH nanoparticles and CG-VV-LDH nanosheets.

Conclusion

In this study, new CG-VV-LDH hybrid nanosheets with active targeting to PepT-1 were prepared and applied for ocular drug

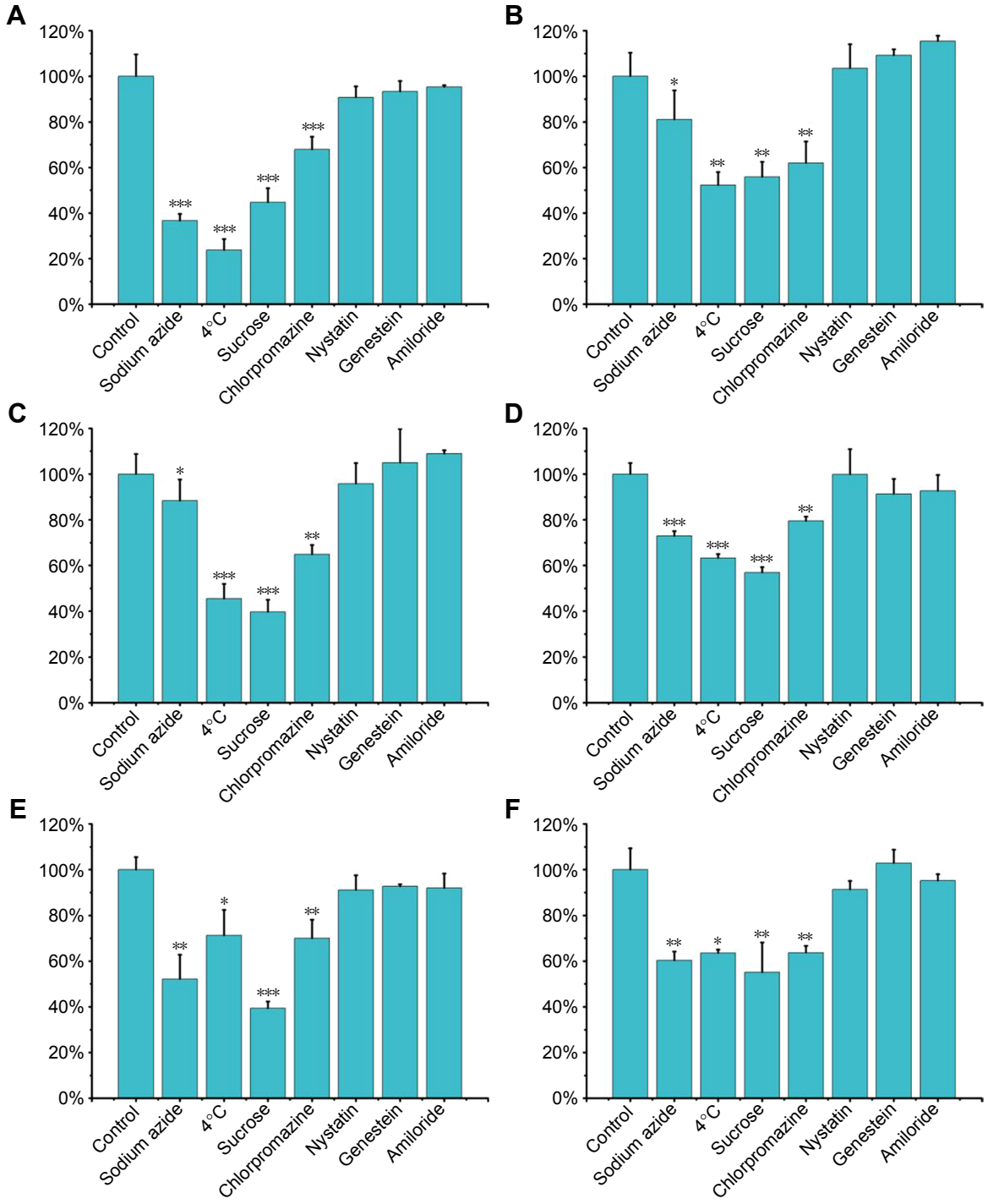

Figure 7 Flow cytometry measurement of intracellular uptake of (**A**) FITC-LDH nanoparticles, (**B**) CG-VV-FITC-LDH nanoparticles, (**C**) CG-VV-FITC-LDH nanosheets treated with specific endocytic inhibitors on HCEpiC; flow cytometry measurement of intracellular uptake of (**D**) FITC-LDH nanoparticles, (**E**) CG-VV-FITC-LDH nanoparticles, (**F**) CG-VV-FITC-LDH nanosheets treated with specific endocytic inhibitors on ARPE-19 cells.

Notes: HCEpiC or ARPE-19 cells without treatment with specific endocytic inhibitors were taken as the control (*$P<0.05$, **$P<0.01$, ***$P<0.001$ vs control group, n=3).

Abbreviations: FITC, fluorescein isothiocyanate; LDH, layered double hydroxide; CG-VV, chitosan–glutathione–valine–valine; HCEpiC, human corneal epithelial primary cells; ARPE-19, retinal pigment epithelial.

delivery. The results of particle size, zeta potential, XRD and TEM confirmed the formation of CG-VV-LDH hybrid nanosheets. CG-VV-LDH hybrid nanosheets were compared with CG-VV-LDH hybrid nanoparticles in several aspects. Both of these two types of LDH nanocomposites showed a sustained release in vitro and prolonged precorneal retention time in vivo. Under in vitro corneal permeation, CG-VV-LDH hybrid nanoparticles showed better permeability. For the first time, HCEpiC and ARPE-19 cells were used in the comparison of these two types of nanocomposites. In MTT assay,

a safe level of LDH concentration at 75 μg/mL was confirmed. According to the results of in vitro corneal permeation and cellular uptake on HCEpiC, the permeation of CG-VV-LDH hybrid nanoparticles was superior to that of CG-VV-LDH hybrid nanosheets even though the content of CG-VV in CG-VV-LDH hybrid nanosheets was ~21 times higher than that in CG-VV-LDH hybrid nanoparticles. The mechanism of cellular uptake of CG-VV-LDH hybrid nanosheets and CG-VV-LDH hybrid nanoparticles on HCEpiC and ARPE-19 cells was clathrin-mediated endocytosis and active transport of PepT-1, which showed that the multifunctionality of these two types of nanocomposites. In summary, based on this study and our previous studies of LDH nanocomposites, the CG-VV-LDH nanoparticle may be a promising carrier for the treatment of ocular diseases of mid-posterior segments due to superior permeability while the CG-VV-LDH nanosheet with prolonged precorneal retention may be suitable for the treatment of ocular surface diseases. Further study would be focused on the differences between CG-VV-LDH hybrid nanoparticles and CG-VV-LDH hybrid nanosheets on ARPE-19 cells.

Acknowledgments

This work was supported by the National Science and Technology of China for the development of new drugs (No 81373362) and the fundamental research funds for the Central Universities of China (No PT2014YX0054).

Disclosure

The authors report no conflicts of interest in this work.

References

1. Gaudana R, Ananthula HK, Parenky A, Mitra AK. Ocular drug delivery. *AAPS J*. 2010;12(3):348–360.
2. Reimondez-Troitiño S, Csaba N, Alonso MJ, de la Fuente M. Nanotherapies for the treatment of ocular diseases. *Eur J Pharm Biopharm*. 2015;95(pt B):279–293.
3. Hoyo CD. Layered double hydroxides and human health: an overview. *Appl Clay Sci*. 2007;36(1–3):103–121.
4. Wang Q, O'Hare D. Recent advances in the synthesis and application of layered double hydroxide (LDH) nanosheets. *Chem Rev*. 2012;112(7):4124–4155.
5. Kuthati Y, Kankala RK, Lee CH. Layered double hydroxide nanoparticles for biomedical applications: current status and recent prospects. *Appl Clay Sci*. 2015;112–113:100–116.
6. Balcomb B, Singh M, Singh S. Synthesis and characterization of layered double hydroxides and their potential as nonviral gene delivery vehicles. *ChemistryOpen*. 2015;4(2):137–145.
7. Alexandre M, Dubois P. Polymer-layered silicate nanocomposites: preparation, properties and uses of a new class of materials. *Mater Sci Eng*. 2000;28(1–2):1–63.
8. Cao F, Wang YJ, Ping QN, Liao ZG. Zn-Al-NO_3-layered double hydroxides with intercalated diclofenac for ocular delivery. *Int J Pharm*. 2011;404(404):250–256.
9. Qin ZG, Zhang J, Chi HB, Cao F. Organic–inorganic hybrid nanocomposites based on chitosan derivatives and layered double hydroxides with intercalated phacolysin as ocular delivery system. *J Nanopart Res*. 2015;17(12):1–15.
10. Xu TT, Zhang J, Chi HB, Cao F. Multifunctional properties of organic-inorganic hybrid nanocomposites based on chitosan derivatives and layered double hydroxides for ocular drug delivery. *Acta Biomater*. 2016;36:152–163.
11. Kuo YM, Kuthati Y, Kankala RK, et al. Layered double hydroxide nanoparticles to enhance organ-specific targeting and the anti-proliferative effect of cisplatin. *J Mater Chem B*. 2015;3(17):3447–3458.
12. Tokudome Y, Morimoto T, Tarutani N, et al. Layered double hydroxide nanoclusters: aqueous, concentrated, stable, and catalytically active colloids toward green chemistry. *ACS Nano*. 2016;10(5):5550–5559.
13. Wang JY, Bao WL, Umar A, Wang Q, O'Hare D, Wan YL. Delaminated layered double hydroxide nanosheets as an efficient vector for DNA delivery. *J Biomed Nanotechnol*. 2016;12(5):922–933.
14. Chi HB, Xu TT, Chen HY, Cao F. Ophthalmic solution of pirenoxine sodium-layered double hydroxide nanosheets and intercalated nanoparticles. *J China Pharm Univ*. 2016;47(4):448–456.
15. Li Y, Chen W, Zhu XY, et al. Folic acid conjugated self-assembled layered double hydroxide nanoparticles for high-efficacy-targeted drug delivery. *Chem Commun (Camb)*. 2013;49(93):10938–10940.
16. Wang L, Wang CY, Liu Q, et al. PEPT1- and OAT1/3-mediated drug-drug interactions between bestatin and cefixime in vivo and in vitro in rats, and in vitro in human. *Eur J Pharm Sci*. 2014;63:77–86.
17. Cao F, Gao YH, Wang M, Fang L, Ping QN. Propylene glycol-linked amino acid/dipeptide diester prodrugs of oleanolic acid for PepT1-mediated transport: synthesis, intestinal permeability, and pharmacokinetics. *Mol Pharm*. 2013;10(4):1378–1387.
18. Cao F, Jia JH, Yin Z, et al. Ethylene glycol-linked amino acid diester prodrugs of oleanolic acid for PepT1-mediated transport: synthesis, intestinal permeability and pharmacokinetics. *Mol Pharm*. 2012;9(8):2127–2135.
19. Xiang CD, Batugo M, Gale DC, et al. Characterization of human corneal epithelial cell model as a surrogate for corneal permeability assessment: metabolism and transport. *Drug Metab Dispos*. 2009;37(5):992–998.
20. Vadlapatla RK, Vadlapudi AD, Ponnaluri VK, Pal D, Mukherji M, Mitra AK. Molecular expression and functional activity of efflux and influx transporters in hypoxia induced retinal pigment epithelial cells. *Int J Pharm*. 2013;454(1):444–452.
21. Vellonen KS, Malinen M, Mannermaa E, et al. A critical assessment of in vitro tissue models for ADME and drug delivery. *J Control Release*. 2014;190:94–114.
22. Zhou Y, Hu Y, Zeng N, et al. Noninvasive monitoring of Pirenoxine Sodium concentration in aqueous humor based on dual-wavelength iris imaging technique. *Biomed Opt Express*. 2011;2(2):231–242.
23. Musumeci AW, Mortimer GM, Butler MK, Xu ZP, Minchin RF, Martin DJ. Fluorescent layered double hydroxide nanoparticles for biological studies. *Appl Clay Sci*. 2010;48(1–2):271–279.
24. Hibino T. A new method for preparation of nanoplates of Zn-Al layered double hydroxides. *Appl Clay Sci*. 2011;54(1):83–89.
25. Shi S, Zhang Z, Luo Z, et al. Chitosan grafted methoxy poly(ethylene glycol)-poly(ε-caprolactone) nanosuspension for ocular delivery of hydrophobic diclofenac. *Sci Rep*. 2015;5:11337.
26. Kang HL, Huang GL, Ma SL, et al. Coassembly of inorganic macromolecule of exfoliated LDH nanosheets with cellulose. *J Phys Chem C*. 2009;113(21):9157–9163.
27. Kang H, Shu Y, Li Z, et al. An effect of alginate on the stability of LDH nanosheets in aqueous solution and preparation of alginate/LDH nanocomposites. *Carbohydr Polym*. 2014;100(2):158–165.
28. Gu Z, Zuo HL, Li L, Wu A, Xu ZP. Pre-coating layered double hydroxide nanoparticles with albumin to improve colloidal stability and cellular uptake. *J Mater Chem B*. 2015;3(16):3331–3333.
29. Agarwal P, Rupenthal ID. In vitro and ex vivo corneal penetration and absorption models. *Drug Deliv Transl Res*. 2016;6(6):634–647.
30. Choi SJ, Choy JH. Layered double hydroxide nanoparticles as target-specific delivery carriers: uptake mechanism and toxicity. *Nanomedicine*. 2011;6(5):803–814.
31. Lajunen T, Nurmi R, Kontturi L, et al. Light activated liposomes: functionality and prospects in ocular drug delivery. *J Control Release*. 2016:doi:10.1016/j.jconrel.2016; 244(B):157–166.

32. Suen WL, Chau Y. Specific uptake of folate-decorated triamcinolone-encapsulating nanoparticles by retinal pigment epithelium cells enhances and prolongs antiangiogenic activity. *J Control Release*. 2013; 167(1):21–28.
33. Yan L, Li G, Zhang S, et al. Cytotoxicity and genotoxicity of multi-walled carbon nanotubes with human ocular cells. *Chin Sci Bull*. 2013; 58(19):2347–2352.
34. Xu ZP, Niebert M, Porazik K, et al. Subcellular compartment targeting of layered double hydroxide nanoparticles. *J Control Release*. 2008; 130(1):86–94.
35. Oh JM, Choi SJ, Kim ST, Choy JH. Cellular uptake mechanism of an inorganic nanovehicle and its drug conjugates: enhanced efficacy due to clathrin-mediated endocytosis. *Bioconjug Chem*. 2006;17(6): 1411–1417.